JOURNAL OF CATALYSIS **172,** 274–280 (1997)
ARTICLE NO. CA971816

On the Nature of Nonframework Cations in a Zeolitic deNO$_x$ Catalyst

A Synchrotron X-Ray Diffraction and ESR Study of Cu-Ferrierite

Martin P. Attfield, Scott J. Weigel, and Anthony K. Cheetham[1]

Materials Research Laboratory, University of California, Santa Barbara, California 93106

Received October 21, 1996; revised June 24, 1997; accepted June 25, 1997

The location of extra-framework Cu^{2+} cations in the dehydrated copper ion exchanged zeolite, ferrierite, has been determined from the analysis of synchrotron X-ray powder diffraction data ($Cu_{0.023}(Al_{0.065}Si_{0.935})O_2$; space group *Immm*, $a = 18.8101(2)$ **Å,** $b = 14.0930(2)$ **Å,** $c = 7.44527(7)$ **Å,** $V = 1973.67(6)$ **Å^3,** $Z = 36$, $R_{wp} = 9.89\%$, $\chi^2 = 1.12$). **One copper site was found towards the side of the 8-ring window at the intersection of the 10- and 8-ring channels. An electron spin resonance (ESR) spectroscopic study indicates the presence of one Cu^{2+} species in the hydrated sample, which forms two Cu^{2+} species upon evacuation to 200°C, only one of which remains after evacuation to 360°C. This remaining Cu^{2+} species has nonaxial symmetry. The low coordination, but high accessibility, of the cation site provides a possible explanation for the high activity of ferrierite and its related pentasil family members for nitrogen oxide decomposition.**

INTRODUCTION

The removal of nitrogen oxides from automobile exhaust streams has been achieved successfully over the last three decades by use of the three-way catalytic converter (1). However, the increasing drive towards the use of lean-burn engines, which render the conventional three-way catalyst ineffective for NO_x emission, has exacerbated the need for a new effective deNO$_x$ catalyst. At the present time, copper- or cobalt-loaded pentasil zeolite catalysts have been found to display the highest activity towards the decomposition of nitrogen oxides (2).

The particular transition metal exchanged zeolite that is the most active for deNO$_x$ depends on the reaction conditions being used. Cu-ZSM-5 has been found to be the most active for many reactions, including direct decomposition of NO to N_2 and O_2 (3, 4) and the selective catalytic reduction (SCR) of NO by certain hydrocarbons in the presence of excess oxygen (5, 6). Other transition metal exchanged zeolites show significant activity for the same reactions and sometimes even greater activity. For example, Co-ferrierite is the most active catalyst for the decomposition in the presence of methane and excess oxygen (7).

To understand the high activity of these catalysts requires knowledge of the location and coordination of the cations in the zeolite. There are only two reported diffraction studies on the locations of extra-framework transition metal cations in the pentasil zeolites, both involving Ni-ZSM-5 (8, 9). Most information on the locations of the cations in these catalysts has been deduced from indirect spectroscopic measurements (10–12).

Cu-ferrierite materials have been found to be highly active for many of the deNO$_x$ reactions discussed in the literature (13). Ferrierite is well known, both in nature and as a synthetic material (14). The structure was first determined by Vaughan (15) and Kerr (16), although there is still discussion as to the correct symmetry of the material (17–19). The framework of ferrierite (see Fig. 1) is based on 5-ring building units that are stacked parallel to the [001] direction. The connection of these rings forms an oval 10-ring channel (pore dimensions 4.2 by 5.4 Å) running along the [001] direction, which is intersected by an 8-ring channel (pore dimensions 3.5 by 4.8 Å) that runs along the [010] direction. The 8-ring channel may also be considered as consisting of cages, bounded by 6-rings and 8-rings, that connect the 10-ring channels. The only extra-framework cation locations reported for ferrierite are those of the alkali metals and alkaline earth metals (15, 18, 20–22).

In this work, we use high resolution synchrotron X-ray diffraction data and ESR spectroscopy to determine the location and coordination of the extra-framework copper cations in a high silica Cu-ferrierite sample.

METHODS

The hydrothermal crystallization of the aluminosilicate ferrierite was carried out in a Teflon-lined 125 ml Parr digestion bomb, according to a modified version of the method used by Kuperman *et al.* (23). The reactants used were pyridine (Fisher, pyr), propylamine (Kodak, $PrNH_2$),

[1] To whom correspondence should be addressed. E-mail: cheetham@iristew.ucsb.edu.

0021-9517/97 $25.00

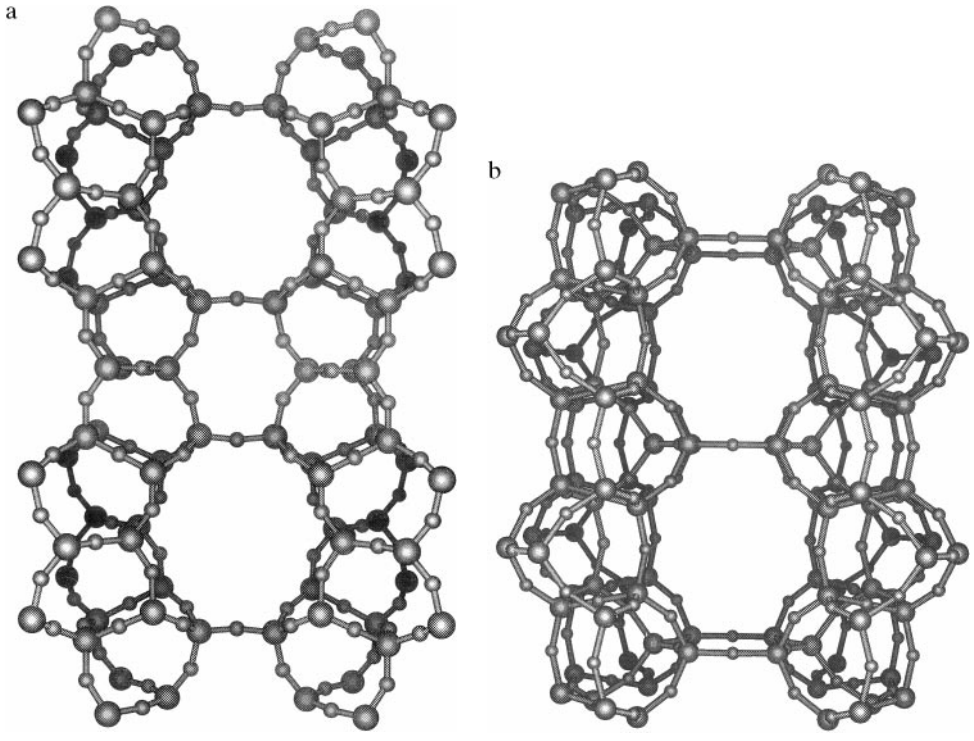

FIG. 1. The structure of ferrierite viewed (a) down the [001] direction showing the 10-ring channel and (b) down the [010] direction showing the 8-ring channel.

HF/pyridine (70 wt% HF, Aldrich), Cab-O-Sil (Kodak M-5, scintillation grade), aluminum sulfate (Aldrich), potassium nitrate (Fisher), and distilled water. The aluminum sulfate was first dissolved in two-thirds of the water. The balance of the water, propylamine, pyridine, and HF/pyridine were mixed together in the Teflon liner and stirred for 5 min. After the amines were mixed thoroughly, potassium nitrate was added and stirred until it dissolved. The silica was added slowly to this mixture while being continuously stirred. The cloudy potassium silicate gel was stirred for an additional hour before the aluminum sulfate solution was added. The resulting aluminosilicate gel was then stirred for $3\frac{1}{2}$ h to ensure that an homogeneous gel was obtained. The initial mole ratio of oxides was

$$K_2O : 8.5\,SiO_2 : Al_2O_3 : 10.8\,HF/pyr : 21.6\,PrNH_2 : 89.2\,pyr : 135\,H_2O.$$

The autoclave was heated to 170°C in a forced draft oven and kept at this temperature for 7 days. After the hydrothermal treatment, the autoclave was removed from the oven and quenched in cold water. The resulting zeolite was separated from the mother liquor by vacuum filtration, washed in deionized water, rinsed in acetone, and dried at room temperature.

The ferrierite isolated from the synthesis was ion-exchanged twice in a 1.0 *M* solution of NH_4NO_3 (Aldrich) before being calcined under a 99% oxygen atmosphere, flow rate 150 $cm^3\ min^{-1}$ in a Lindberg muffle furnace that was ramped at 2°C min^{-1} from room temperature to 550°C and held at temperature for 12 h. A gram of the resulting colorless ferrierite was then ion-exchanged overnight in 100 mL of 1.0 *M* NH_4NO_3 solution a total of three times. In between exchanges the ferrierite was washed in 200 mL of deionized water. The ammonium exchanged ferrierite was then refluxed five times overnight in a 0.5 *M* $Cu(NO_3)_2$ (Aldrich) solution (1 g of ferrierite per 50 mL of solution). The pH of the solution remained at ~4 during the copper exchanges. The sample was washed in 200 mL of deionized water between refluxes and in 500 mL at the end of the treatment. The Cu-ferrierite resulting from this procedure was bluish green in color and had a dehydrated unit cell composition of $Cu_{0.123}(Al_{0.065}Si_{0.935})O_2$ from chemical analysis (Galbraith Laboratories). Preliminary diffraction data collected on a laboratory X-ray diffractometer indicated the presence of a trace amount of an unidentifiable second phase in the sample, which may account for the excess of copper found in the analysis (see below).

A small amount of the sample was heated under a vacuum of 10^{-5} Torr (1 Torr = 133.3 *N* m^{-2}) to a temperature of 360°C at a rate of 1°C min^{-1}. During the ramp to 360°C, the temperature was held at 100°C for 2 h, 175°C for 2 h, and finally at 360°C for 6 h, before being cooled to room temperature at a rate of 2°C min^{-1}. The resulting black

sample was transferred under vacuum to a nitrogen glove box where was it was loaded and sealed in a 0.7-mm diameter Lindemann glass capillary tube.

Room temperature synchrotron X-ray powder diffraction data were collected on beamline X3B1 at the National Synchrotron Light Source, Brookhaven National Laboratory. The mean wavelength used was 1.14879(2) Å and data were collected from 3 to 75° 2θ. The diffractometer was operated in triple axis mode with a Si(111) monochromator and Ge(111) analyzer. The sample was spun during data collection to minimize preferred orientation and sampling effects.

The ESR spectra was collected at 10 K on a Bruker ESP-300 spectrometer operating in the X-band at a frequency of 9.460 GHz. Three samples of the polycrystalline Cu-ferrierite sample were studied. The first sample was untreated (raw). The second sample was heated to 200°C under vacuum (10^{-4} Torr). The heating rate was 1°C min^{-1} and the sample was held at 100°C for 2 h before reaching 200°C, where it was held at temperature for 6 h. The last sample underwent a similar dehydration treatment to the second but the maximum temperature it was exposed to was 360°C for a time of 4 h. All three samples were loaded into 4-mm o.d. quartz ESR tubes, evacuated (10^{-6} Torr) for 10 min and sealed under vacuum. The two dehydrated samples were loaded into the ESR tubes in a nitrogen-filled glovebox and the ESR tubes were fitted with a tap so they could be transferred to the vacuum line for sealing without exposure to air. The calibration standard used was DPPH, which gave a *g*-value of 2.008. The observed ESR spectra were simulated using the program POWDER (24).

RESULTS

Prior inspection of the synchrotron X-ray diffraction pattern indicated the presence of two phases, ferrierite and copper (II) oxide, in the sample. The synchrotron X-ray data were initially fitted using the Le Bail method (25) to obtain accurate lattice parameters and profile coefficients for the two phases. Profile analysis was performed on 12,182 data points in the range 13 to 75° 2θ, thus excluding the first seven highly asymmetrical peaks in the pattern. The profile of the ferrierite phase showed signs of peak broadening which was accounted for by including terms in the pseudo-Voigt peak shape that allowed for anisotropic particle size broadening and broadening due to the presence of stacking faults along the (110) plane, as previously reported by Sanders (26) and Gramlich-Meier *et al.* (20).

The lattice parameters and profile coefficients obtained from the Le Bail fit were used in the subsequent Rietveld refinement (27). The starting model for the ferrierite framework was taken from the neutron powder refinement by Pickering *et al.* (21), using the space group *Immm*; there was no evidence for a lowering of symmetry to space group Pmnn as seen by Morris *et al.* (19). The model for the other phase in the refinement, Cu(II)O, was taken from the crystal structure by Ashbrink *et al.* (28).

Initial refinement of the framework gave a chemically unreasonable range of T–O bond distances, so restraints on the bond distances were used. A T–O bond length of 1.61 ± 0.01 Å was imposed on the framework, based on a weighted value of the Si–O (1.60 Å) and Al–O (1.74 Å) bond distances. The soft constraint common-weight factor was adjusted so that all the framework T–O bond lengths remained at chemically sensible values during refinement. One extra-framework position was found from subsequent difference Fourier syntheses. This was refined as a Cu^{2+} cation as the bond distances to framework oxygen atoms were characteristic of Cu–O bonds found in other Cu^{2+} containing compounds. Addition of the Cu^{2+} cation to the refinement enabled the common-weight factor on the T–O bond length constraints to be reduced while keeping all the T–O bond lengths within a reasonable range. The final cycle of least-squares refinement included terms for the diffractometer zero point, the lattice parameters of both phases, the phase fractions of the two phases, all the atomic positions, the occupancy factors of the extra-framework Cu^{2+} cation and the isotropic temperature factors of the framework atoms in ferrierite. The isotropic temperature factors of the extra-framework Cu^{2+} cation and the atoms in the CuO phase were held at reasonable values. The Si/Al ratio of the ferrierite was included in the refinement by considering the T site atoms to have a 0.065 occupancy of Al and a 0.935 occupancy of Si. The final observed, calculated and difference plots are shown in Fig. 2. Details of the refinement are given in Table 1, final atomic positions, occupancies and temperature factors are given in Table 2, and selected bond distances and angles are given in Tables 3 and 4.

TABLE 1

Crystallographic Data for the Synchrotron X-Ray Refinement of Dehydrated Cu-Ferrierite and Copper Oxide

Molecular formula	$Cu_{0.017}(Al_{0.065}Si_{0.935})O_2$		CuO
Molecular weight	61.092		79.545
Formula units per unit cell	36		4
a (Å)	18.8101(2)		4.680(1)
b (Å)	14.0929(2)		3.4325(7)
c (Å)	7.44527(7)		5.134(1)
β (°)	—		99.25(1)
V (Å^3)	1973.65(6)		81.40(1)
Space group	*Immm (#71)*		*C2/c(15)*
Weight fraction	87.93		12.07
R_{wp} [a]	9.98	R_p [b]	7.64
χ^2 [c]	1.142	*N*	12182
P	49	*C*	16

[a] $R_{wp} = 100\{\Sigma w_i(y_i - y_{ci})^2 / \Sigma w_i y_i^2\}^{1/2}$.

[b] $R_p = 100\Sigma|y_i - y_{ci}| / \Sigma|y_i|$.

[c] $\chi^2 = \{\Sigma w_i(y_i - y_{ci})^2/(N-P-C)\}$, where y_i, y_{ci}, and w_i are the observed intensity, calculated intensity, and weight for the *i*th step, *N* is the number of data points, *P* is the number of parameters, and *C* is the number of constraints applied.

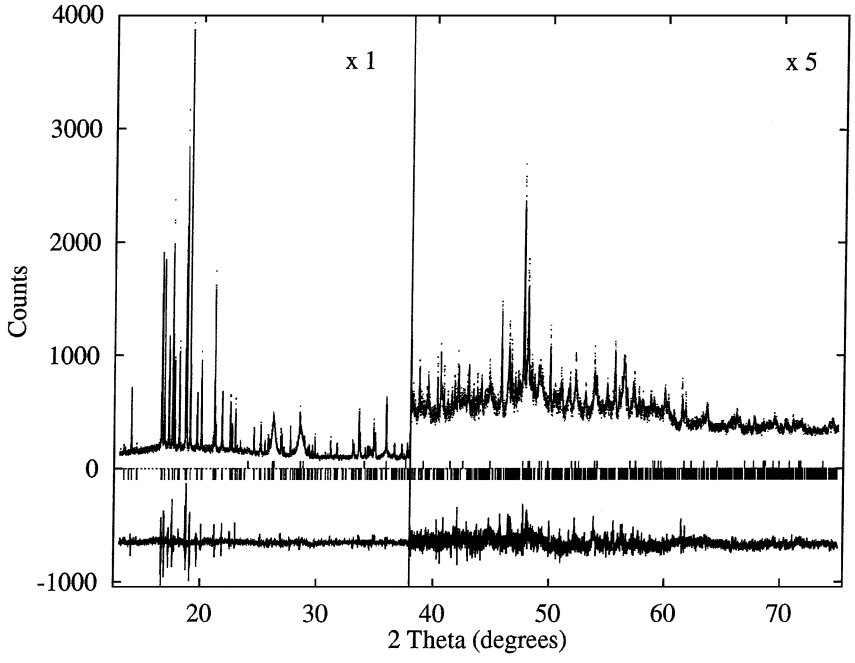

FIG. 2. The observed (dots), calculated (solid), and difference plot for the Rietveld refinement of dehydrated Cu-ferrierite and copper oxide. Reflection positions are shown as ticks for the Cu-ferrierite (upper) and copper oxide (lower). The high angle portion of the pattern is magnified fivefold.

All Rietveld and Le Bail refinements were performed using the GSAS suite of programs (29).

The composition of the Cu-ferrierite phase calculated from the refinement is $Cu_{0.023}(Al_{0.065}Si_{0.935})O_2$ (the Si/Al ratio is assumed to be that given by the chemical analysis). The ratio of the two phases Cu-ferrierite/CuO, given by the refinement, is 9.676. Thus, the total Cu/T site ratio of the bulk sample is 0.128 which is in excellent agreement with that given by the chemical analysis (0.123). Since the number of extra-framework Cu^{2+} cations in the zeolite is not enough to counterbalance the framework charge of the zeolite, the remainder of the charge is presumably compensated by the presence of Brønsted acid sites produced during the thermal decomposition of residual NH_4^+ cations. The large amount of CuO formed is likely to have arisen from the thermal treatment of copper in the small amount of the unidentifiable second phase initially present in the sample or from surface copper hydroxyl species.

The location of the extra-framework Cu^{2+} cation is shown in Fig. 3. The Cu^{2+} cation site, Cu(1), is situated at the edge

TABLE 2

Final Atomic Coordinates, Isotropic Temperature Factors, and Occupancy Factors of Dehydrated Cu-Ferrierite and Copper Oxide

Atom	*x*	*y*	*z*	Uiso (Å^2)	Occupancy
Cu-ferrierite					
T(1)	0.1527(3)	0.0000	0.0000	0.020(2)	1.000
T(2)	0.0833(2)	0.2000(4)	0.0000	0.021(1)	1.000
T(3)	0.2717(2)	0.0000	0.2931(6)	0.019(1)	1.000
T(4)	0.3239(1)	0.2013(2)	0.2104(4)	0.0198(9)	1.000
O(1)	0.0000	0.2104(9)	0.0000	0.043(5)	1.000
O(2)	0.2444(6)	0.0000	0.5000	0.027(5)	1.000
O(3)	0.0979(4)	0.0882(5)	0.0000	0.055(4)	1.000
O(4)	0.2049(4)	0.0000	0.1701(9)	0.038(4)	1.000
O(5)	0.2500	0.2500	0.2500	0.036(3)	1.000
O(6)	0.1588(5)	0.2826(5)	0.5000	0.046(4)	1.000
O(7)	0.1149(3)	0.2519(4)	0.1750(7)	0.044(3)	1.000
O(8)	0.3198(3)	0.0895(3)	0.2480(9)	0.024(2)	1.000
Cu(1)	0.576(2)	0.302(2)	0.064(4)	0.025	0.038(2)
Copper oxide					
Cu(1)	0.2500	0.2500	0.0000	0.025	1.000
O(1)	0.0000	−0.556(3)	0.2500	0.025	1.000

TABLE 3

Selected Bond Distances (Å) for Dehydrated Cu-Ferrierite and Copper Oxide

Cu-ferrierite			
T(1)−O(3)	1.614(5)	T(1)−O(3)	1.614(5)
T(1)−O(4)	1.602(5)	T(1)−O(4)	1.602(5)
T(2)−O(1)	1.573(4)	T(2)−O(3)	1.599(6)
T(2)−O(7)	1.609(4)	T(2)−O(7)	1.609(4)
T(3)−O(2)	1.623(4)	T(3)−O(4)	1.555(5)
T(3)−O(8)	1.588(4)	T(3)−O(8)	1.588(4)
T(4)−O(5)	1.578(3)	T(4)−O(6)	1.616(4)
T(4)−O(7)	1.578(4)	T(4)−O(8)	1.601(4)
Cu(1)−O(6)	2.03(3)	Cu(1)−O(7)	2.21(3)
Cu(1)−T(4)	2.60(3)		
Copper oxide			
Cu(1)−O(1) × 2	1.907(5)	Cu(1)−O(1) × 2	1.985(3)

TABLE 4

Selected Bond Angles (°) for Dehydrated Cu-Ferrierite and Copper Oxide

Cu-ferrierite			
O(3)–T(1)–O(3)	100.7(7)	O(3)–T(1)–O(4)	113.02(23)
O(3)–T(1)–O(4)	113.02(23)	O(3)–T(1)–O(4)	113.02(23)
O(3)–T(1)–O(4)	113.02(23)	O(4)–T(1)–O(4)	104.5(7)
O(1)–T(2)–O(3)	105.3(7)	O(1)–T(2)–O(7)	109.0(4)
O(1)–T(2)–O(7)	109.0(4)	O(3)–T(2)–O(7)	112.6(4)
O(3)–T(2)–O(7)	112.6(4)	O(7)–T(2)–O(7)	108.2(6)
O(2)–T(3)–O(4)	107.7(5)	O(2)–T(3)–O(8)	112.4(4)
O(2)–T(3)–O(8)	112.4(4)	O(4)–T(3)–O(8)	109.58(34)
O(4)–T(3)–O(8)	109.58(34)	O(8)–T(3)–O(8)	105.2(5)
O(5)–T(4)–O(6)	107.3(4)	O(5)–T(4)–O(7)	111.06(34)
O(5)–T(4)–O(8)	110.65(27)	O(6)–T(4)–O(7)	108.6(5)
O(6)–T(4)–O(8)	108.6(5)	O(7)–T(4)–O(8)	110.6(4)
T(2)–O(1)–T(2)	169.3(11)	T(3)–O(2)–T(3)	143.2(8)
T(1)–O(3)–T(2)	150.3(7)	T(1)–O(4)–T(3)	163.9(7)
T(4)–O(5)–T(4)	180.0	T(4)–O(6)–T(4)	151.6(7)
T(2)–O(7)–T(4)	153.9(6)	T(3)–O(8)–T(4)	147.8(4)
O(6)–Cu(1)–O(7)	75.3(10)		
Copper oxide			
O(1)–Cu(1)–O(1) × 2	83.63(7)	O(1)–Cu(1)–O(1) × 2	96.37(7)
O(1)–Cu(1)–O(1)	179.972	O(1)–Cu(1)–O(1)	180.0

TABLE 5

ESR Parameters of Cu^{2+} in Cu-Ferrierite at 10 K

Treatment	$g_{\parallel(zz)}$	$A_{\parallel(zz)}$ (10^{-4} cm^{-1})	$g_{\perp(yy)}$	$A_{\perp(yy)}$ (10^{-4} cm^{-1})	$g_{\perp(xx)}$
Raw	2.397	150	2.076	—	—
200°C	2.412	125	2.080	—	—
	2.330	176	2.065	8	—
360°C	2.330	175	2.069	18	2.056
Standard					
DPPH	2.008	—	—	—	—

of the 8-ring window at the intersection of the 10- and 8-ring channels. The Cu(1) has two short bonds to framework oxygen atoms of 2.03(3) and 2.21(3) Å. The bond lengths are in good agreement with those seen for other extra-framework Cu^{2+} cation sites in dehydrated zeolites, e.g., Cu-zeolite-A (Cu–O distances 2.138 Å) (30), Cu-chabazite (Cu–O distance 1.965 Å) (31) and Cu-faujasite (Cu–O distances 2.12 to 2.77 Å) (32). The coordination of the Cu(1) site by the two framework oxygen atoms is not the first example of such low coordination in zeolites. Similar coordination has been found for Cu^{2+} cations in the SIII site of faujasite, where distances to two framework oxygen atoms of 2.16(7) and 2.77(7) Å were reported (32). The occupancy of the Cu(1) site is low enough to assume that two adjacent sites are never occupied simultaneously. Simultaneous occupation by two cations would be physically unreasonable because of their close proximity to one another.

The observed and simulated ESR spectra of the sample after the different thermal treatments are shown in Fig. 4 and the values of g and A for all three samples are given in Table 5. The spectrum of the raw material contains a broad

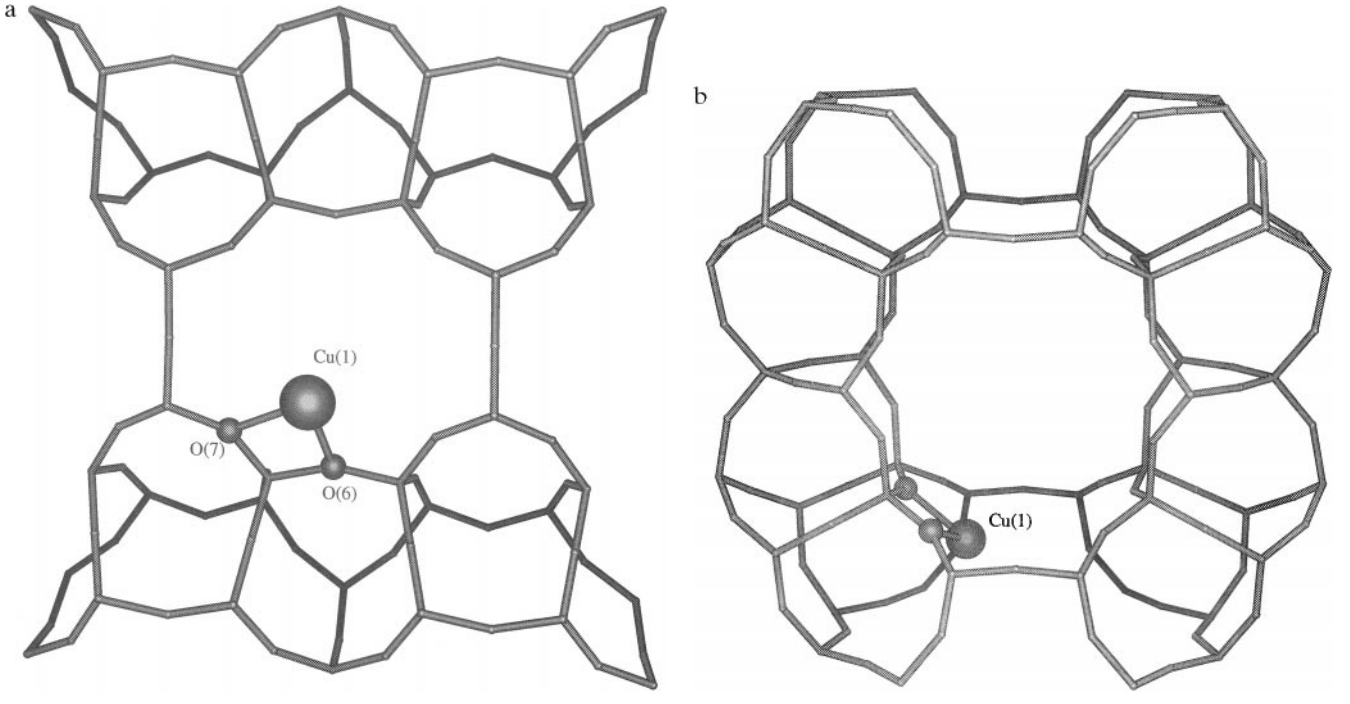

FIG. 3. Location of the extra-framework Cu^{2+} cations in the Cu-ferrierite viewed (a) down the [010] direction and (b) down the [001] direction.

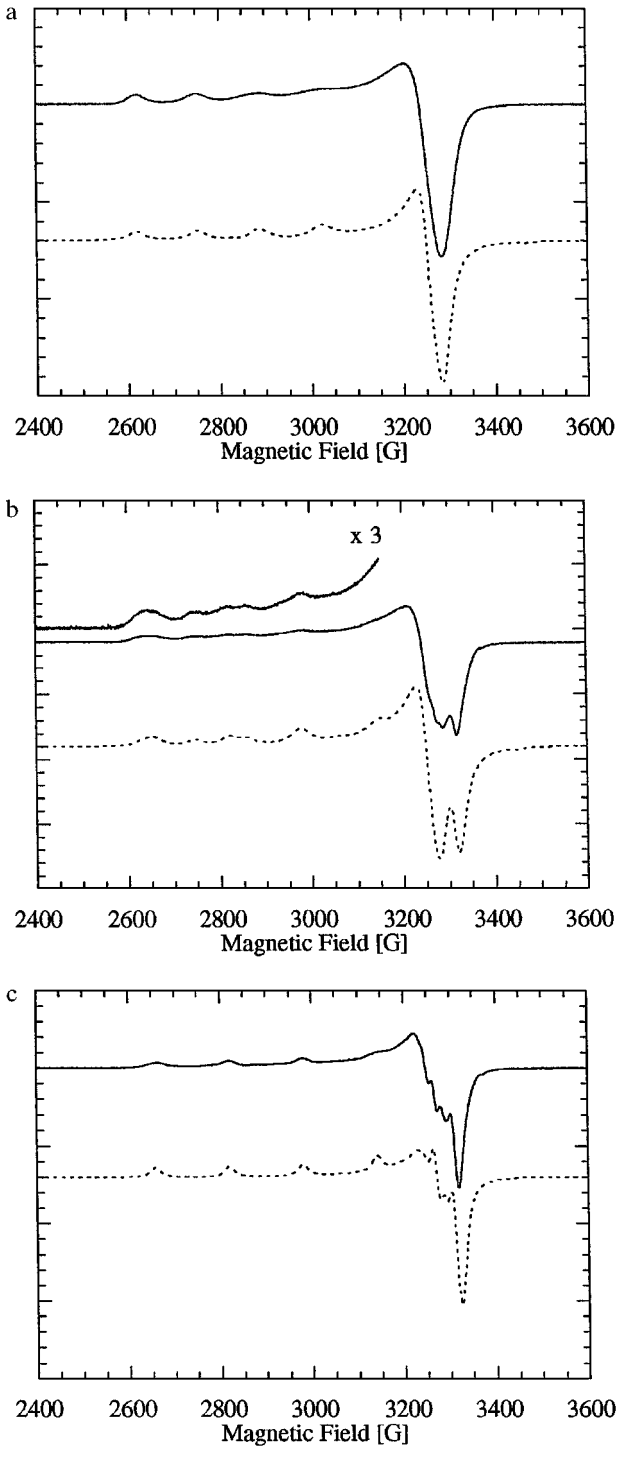

FIG. 4. Experimental (solid) and simulated (dashed) ESR spectra for Cu-ferrierite (a) hydrated, (b) dehydrated at 200°C, and (c) dehydrated at 360°C.

signal indicative of one Cu^{2+} species with ESR parameters of $g_{\|} = 2.397$, $A_{\|} = 150 \times 10^{-4}$ cm^{-1}, and $g_{\perp} = 2.076$. These results are typical for hydrated Cu^{2+} cations; a similar spectrum and parameters are found for hydrated Cu-ZSM-5 ($g_{\|} = 2.379$, $A_{\|} = 153 \times 10^{-4}$ cm^{-1}, and $g_{\perp} = 2.076$) (33). This Cu^{2+} species is assumed to be $[Cu(H_2O)_6]^{2+}$. On dehydration to 200°C, two Cu^{2+} species are observable in the spectrum. One species has ESR parameters of $g_{\|} = 2.4212$, $A_{\|} = 125 \times 10^{-4}$ cm^{-1}, and $g_{\perp} = 2.080$, the other has ESR parameters of $g_{\|} = 2.330$, $A_{\|} = 176 \times 10^{-4}$ cm^{-1}, $g_{\perp} = 2.065$, and $A_{\perp} = 8 \times 10^{-4}$ cm^{-1}. The Cu^{2+} species with the higher $g_{\|}$ value is presumably Cu^{2+} with a different environment or degree of hydration and the other Cu^{2+} species is likely to be a more dehydrated Cu^{2+} cation. Only one Cu^{2+} species is found in the spectrum of the sample dehydrated to 360°C, which has the ESR parameters of $g_{\|(zz)} = 2.330$, $A_{\|(zz)} = 175 \times 10^{-4}$ cm^{-1}, $g_{\perp(yy)} = 2.069$, $A_{\perp(yy)} = 18 \times 10^{-4}$ cm^{-1}, and $g_{\perp(xx)} = 2.056$. This species has the same ESR parameters as the second species in the sample dehydrated to 200°C, the values of $g_{\perp}$ and $A_{\perp}$ for the former are more accurate as this part of the spectrum is more clearly resolved.

The ESR results shows there is only one Cu^{2+} species remaining in the Cu-ferrierite after dehydration to 360°C, in agreement with the findings from our X-ray diffraction work. This species is present at 200°C, as indicated by its occurrence in the ESR spectrum of the sample dehydrated at this temperature. The ESR parameters of this species lie in the range found for other dehydrated Cu^{2+} species in various zeolites (11, 12, 33–36), but are not identical to any of those reported previously. The nonaxial symmetry exhibited by the Cu^{2+} species found in the ferrierite is in agreement with the low site symmetry of the Cu^{2+} cation found from the diffraction analysis.

DISCUSSION

The Cu^{2+} cation site in the dehydrated Cu-ferrierite is found to the side of the 8-ring at the intersection of the 10- and 8-ring channels. The cation siting can be explained if we assume that the $[Cu(H_2O)_6]^{2+}$ species, as found from the ESR study, is found in the main channel between the 8-rings or at the center of the cage that forms part of the 8-ring channel. An analogous octahedral Mg^{2+} species ($Mg–O_{aq}$ distances 1.99 to 2.11 Å) has been found in the latter location in room temperature crystal structures of natural ferrierite (15, 18, 20). Upon heating, water molecules are removed from the coordination sphere of the Cu^{2+} cations and, by 200°C, fully dehydrated and partially dehydrated Cu^{2+} species coexist. At 360°C, all the Cu^{2+} cations will have lost their coordinated water molecules and migrated to the framework to find the highest possible coordination environment available. The position found for the Cu^{2+} cation requires the least movement of the Cu^{2+} cations from either of the locations in which the $[Cu(H_2O)_6]^{2+}$ species was likely to be present initially and migration should occur readily. The Cu^{2+} cations are assumed to remain in this oxidation state because Cu^{+} cations are not observable by ESR spectroscopy and the Cu–O distances in the structure are those expected for Cu^{2+} cations.

The location found for the Cu^{2+} cation site reveals that it is poorly coordinated, but extremely accessible to all reactant molecules passing through the channels. The low coordination of the Cu^{2+} cations makes them more susceptible to redox chemistry, when exposed to NO, than a highly coordinated Cu^{2+} cation. Unlike faujasite catalysts, where most of the Cu^{2+} cation sites are situated in inaccessible positions within the sodalite cage (32, 37), the cation location in the ferrierite means that the NO and many of the hydrocarbon molecules can access the active centers easily. Thus, the presence of the poorly coordinated but highly accessible Cu^{2+} cations makes Cu-ferrierite a very active $deNO_x$ catalyst. The above reasoning could be extended to other zeolites of the pentasil family that are active $deNO_x$ catalysts, such as ZSM-5 and mordenite (38); since these zeolites have few cation sites within inaccessible cavities in their structures, most extra-framework transition metal cations should be poorly coordinated but highly accessible to reactant molecules.

ACKNOWLEDGMENTS

The work was funded by the MRL program of the National Science Foundation under award DMR 9123048 and Los Alamos National Laboratory. Research carried out (in part) at the National Synchrotron Light Source, Brookhaven National Laboratory, which is supported by the U.S. Department of Energy, Division of Materials Sciences and Division of Chemical Sciences. We thank Peter Stephens for collecting the synchrotron X-ray data at the SUNY X3B1 beamline, which is supported by DOE Office of Basic Energy Sciences under Grant DE-FG0286-ER45231.

REFERENCES

1. Bond, G. C., "Heterogeneous Catalysis, Principles and Applications." Oxford Univ. Press, Oxford, 1987.
2. Shelef, M., *Chem. Rev.* **95**, 209 (1995).
3. Iwamoto, M., Furukawa, H., Mine, Y., Uemura, F., Mikuriya, S., and Kagawa, S., *J. Chem. Soc., Chem. Commun.* 1272 (1986).
4. Li, Y., and Hall, W. K., *J. Phys. Chem.* **94**, 6145 (1990).
5. Iwamoto, M., Yahiro, H., Shundo, Y., Yu-u, Y., and Mizuno, M., *Shokbai (Catalyst)* **32**, 430 (1990).
6. Iwamoto, M., and Hamada, H., *Catal. Today* **10**, 57 (1991).
7. Li, Y., and Armor, J. N., *Appl. Catal. B: Environmental* **3**, L1 (1993).
8. Mentzen, B. F., Sacerdote-Peronnet, M., and Bouix, J., *C.R. Acad. Sci. Paris* **315**, 1073 (1992).
9. Zhenyi, L., Wangjin, Z., Qin, Y., and Guanglie, L., *Stud. Surf. Sci. Catal.* **28**, 415 (1986).
10. Dedecek, D., Sobalik, Z., Tvaruzkova, Z., Kaucky, D., and Wichterlova, B., *J. Phys. Chem.* **99**, 16327 (1995).
11. Kucherov, A. V., Slinkin, A. A., Kondratev, D. A., Bondarenko, T. N., Rubenstein, A. M., and Minachev, Kh. M., *Zeolites* **5**, 320 (1985).
12. Grünert, W., Hayes, N. W., Joyner, R. W., Shapiro, E. S., Rafiq, M., Siddiqui, H., and Baeva, G. N., *J. Phys. Chem.* **98**, 10832 (1994).
13. Iwamoto, M., Yahiro, H., and Mizuno, N., *in* "Proceedings, 9th International Zeolite Conference, Montreal, 1992" (R. von Ballmoos, J. B. Higgins, and M. M. J. Treacy, Eds.), Vol. 2. p. 397, Butterworth-Heinemann, Stoneham, 1992.
14. Wise, W. S., and Tschernich, R. W., *Am. Mineral.* **61**, 60 (1976).
15. Vaughan, P. A., *Acta Crystallogr.* **21**, 983 (1966).
16. Kerr, S., *Nature* **210**, 294 (1966).
17. Gramlich-Meier, R., Gramlich, V., and Meier, W. M., *Am. Mineral.* **70**, 619 (1985).
18. Alberti, A., and Sabelli, C., *Z. Kristallogr.* **178**, 249 (1987).
19. Morris, R. E., Weigel, S. J., Henson, N. J., Bull, L. M., Janicke, M. T., Chmelka, B. F., and Cheetham, A. K., *J. Am. Chem. Soc.* **116**, 11849 (1994).
20. Gramlich-Meier, R., Meier, W. M., and Smith, B. K., *Zeit. Kristallogr.* **169**, 201 (1984).
21. Pickering, I. J., Maddox, P. J., Thomas, J. M., and Cheetham, A. K., *J. Catal.* **119**, 261 (1989).
22. Mortier, W. J., "Compilation of Extra-framework Sites in Zeolites." Butterworth, Guildford, 1982.
23. Kuperman, A., Nadimi, S., Oliver, S., Ozin, G. A., Garces, J. M., and Olken, M. M., *Nature* **365**, 239 (1993).
24. Daul, C., Schlapfer, C. W., Ammeter, J., and Gamp, E., *Comp. Phys. Commun.* **21**, 385 (1981).
25. Le Bail, A., Duroy, H., and Fourquet, J. L., *Mat. Res. Bull.* **23**, 447 (1988).
26. Sanders, J. V., *Zeolites* **5**, 81 (1985).
27. Rietveld, H., *Acta Crystallogr.* **2**, 65 (1969).
28. Ashbrink, S., and Lorrby, L. J., *Acta Crystallogr. B* **24**, 1968 (1982).
29. Larson, A. C., and Von Dreele, R. B., Los Alamos Laboratory Report No. LA-UR-86-748, 1987.
30. Lee, S. H., and Seff, K., *J. Phys. Chem.* **85**, 3978 (1981).
31. Pluth, J. J., Smith, J. V., and Mortier, W. J., *Mat. Res. Bull.* **12**, 1001 (1977).
32. Maxwell, I. E., and de Boer, J. J., *J. Phys. Chem.* **79**, 1875 (1975).
33. Anderson, M. W., and Kevan, L., *J. Phys. Chem.* **91**, 4174 (1987).
34. Sendoda, Y., and Ono, Y., *Zeolites* **6**, 209 (1986).
35. de Travernier, S., and Schoonheydt, R. A., *Zeolites* **11**, 155 (1991).
36. Schoonheydt, R. A., *Catal. Rev. Sci. Eng.* **35**, 129 (1993).
37. Gallezot, P., Ben Taarit, Y., and Imelik, B., *J. Catal.* **26**, 295 (1972).
38. Attfield, M. P., Weigel, S. J., and Cheetham, A. K., *J. Catal.*, in press.